Estimating evapotranspiration over vegetated surfaces based on wet patch patterns

Peiyuan Li and Zhi-Hua Wang

ABSTRACT

Evapotranspiration (ET) is a critical component of the hydrological cycle and natural water-energy nexus. The dynamics of soil water content (θ) in the top surface layer, regulated by local climate, predominates the surface energy exchange and ET behavior. In this study, we proposed a novel ET-θ relation using a physically based wet patch radius coupling the near surface turbulent transfer and soil water availability. The model is tested against the dataset from eddy covariance (EC) sites in the AmeriFlux network. The results show that ET rate is supply-driven under low soil moisture conditions since the plant controls the transpiration rate to conserve water due to water stress. While in energy-limited condition, increasing soil moisture will not promote ET rate as it is bounded by the lower atmospheric demand. The proposed method is practically designed to calculate ET using variables readily measured by standard EC towers such as soil moisture and meteorological measurements. The method can also potentially be extended to predict the spatial and physical patterns of ecosystem services under different hydroclimatic conditions.

Key words | AmeriFlux towers, evapotranspiration, land–atmosphere interactions, soil moisture, vegetated surfaces, wet patches

Peiyuan Li
Zhi-Hua Wang (corresponding author)
School of Sustainable Engineering and the Built Environment,
Arizona State University,
Tempe, AZ 85287,
USA
E-mail: *zhwang@asu.edu*

INTRODUCTION

The actual evapotranspiration (ET) rate over vegetated surfaces is regulated by many factors, including the energy and water availability at the land surface, land cover type, geomorphology, near-surface atmospheric condition, etc. (Brutsaert 1982). The water content in topsoil controls the surface energy exchange and the growth of plants. Hence, the temporal dynamics of soil moisture (θ) usually determine ET over vegetated surfaces. In previous hydrological or ecohydrological studies, ET was formed piece-wise linearly (Wetzel & Chang 1987; Laio *et al.* 2001; Guswa *et al.* 2002; Lu *et al.* 2011) or in power function with soil moisture through statistical approaches based on empirical data (Longobardi & Khaertdinova 2014). However, the geostatistical methods oversimplified the dynamics of ET-θ interactions. Essentially, the spatial and temporal patterns of θ largely depend on the characteristics of the local climate (Lawrence & Hornberger 2007), leading to ET estimation dependent on climate variables such as Bowen ratio and dryness index in the Budyko curve.

While extensive research efforts have been devoted to establish accurate ET-θ relationships, linking the two variables involves a complex of interactions in the soil–vegetation–atmosphere continuum. Practical, and hence, applicable methods therefore need to account for the fine balance between the complexity of real physics, mathematical tractability, and portability to different geographic and climate zones, without significantly compromising the accuracy. In-depth reviews for different types of methods for estimating ET can be found in Xu & Singh (2000, 2001), Kumar *et al.* (2012) and Yang (2015). Conventionally, the most widely used Penman–Monteith (P-M) method (Penman 1948; Monteith 1965) estimates ET for crops and other homogeneous vegetated surfaces by quantifying the surface condition via the surface conductance, which

doi: 10.2166/nh.2019.034

serves as the intermediate parameter and needs to be estimated from the active leaf area index (LAI) and the stomatal conductance. However, stomatal conductance varies from one crop to another depending on plant types, properties, and spatial distribution (Jarvis & McNaughton 1986). Plants under different growing phases and meteorological conditions show different stomatal conductance as well (Buckley & Mott 2013; Buckley 2017), therefore, the accurate estimation of surface conductance remains a challenging task. For example, Li *et al.* (2015) tested 12 surface conductance models in an arid environment and calculated that the model with best accuracy requires six parameters and careful calibration from measured data. On the other hand, the FAO 56 Penman–Monteith equation standardizes the surface conductance, calculating ET over a reference vegetated surface (Allen *et al.* 1998). This method is applicable to other crops by applying a constant crop factor to the reference evapotranspiration (ET_0) rate. Although different crop factors could be chosen during the different growth phases of the plants, this method assumes ET between any other vegetation and the reference crop following a linear relation during the growing season; its applicability is rather limited to crops only.

For non-homogeneous surfaces, ET is considered as a composite of bare soil evaporation and plant transpiration and usually simulated by dual-source models. One dual-source model assumed a semi-transparent canopy layer that covers the bare soil and intercepts a portion of solar radiation, thus reducing the energy input to the soil below (Shuttleworth & Wallace 1985). This model was typically applied to dense vegetated surfaces. Another approach, termed patch model, assumes that both canopy and bare soil receive energy input directly, as the open space over bare soil is sufficient for full energy input when vegetation grows sparsely (e.g., Lhomme *et al.* 1994). The total available energy is then partitioned as proportional to the plant–soil area ratio (Lhomme & Chehbouni 1999). In both cases, E can be estimated using the soil evaporation models, such as those based on Schlünder's drying theory (Schlünder 1988a, 1988b, 2004) over porous media (Haghighi *et al.* 2013); while the plant transpiration is estimated using equivalence between the canopy and an imaginary big leaf, enabling applicability of ET estimate for homogeneous surfaces, e.g., the P-M method. Nevertheless, the dual-source models loosely integrate plant–soil interactions and their applications were still limited to either very dense or sparse vegetation surfaces (Guan & Wilson 2009; Yang 2015). A family of hybrid dual-source models has lately been developed to combine the two basic approaches and is capable of differentiating the inter-canopy soil evaporation from under-canopy soil evaporation. For example, the TVET model (Guan & Wilson 2009) shows good accuracy in partitioning potential evaporation and transpiration, with further modification by Yang (2015). Haghighi & Kirchner (2017) introduced the near-surface turbulence to explore the ET-θ relation under the framework of the hybrid dual-source scheme that used Schlünder's drying theory and a big-leaf transpiration model. However, both the algorithms proposed by Yang (2015) and Haghighi & Kirchner (2017) still relied on the estimation of stomatal and surface conductance.

The demanding data requirement and the uncertainties in parameter estimation of the P-M method and dual-source model stimulated researchers to create more practical methods to calculate ET with reasonable accuracy. A versatile approach is to utilize an extension of the ET-θ relation to calculate ET from potential evapotranspiration (E_p). The ET-θ relation is further quantified by a reduction factor (also called stress factor, ET coefficient in some literature), which accounts for the derivation from the actual water availability and meteorological condition to the potential scenario. E_p can be estimated through multiple well-established methods like Penman (1948), or Thornthwaite equation (Thornthwaite 1948; Thornthwaite & Mather 1955), and Priestley & Taylor (1972). The reduction factor (β) was parameterized by Nappo (1975) on six types of bare soils, Xue *et al.* (1991) on 12 types of vegetated surfaces, and Mintz & Walker (1993) on grass-covered surfaces, using statistical regressions. These studies treated β either as a single variable function of soil wetness or as a multivariable function of relative water content and other meteorological parameters due to their determinative roles in controlling ET. Kurc & Small (2004) compared ET-θ relation with β-θ relation using observation data over grassland and shrubland during the monsoon seasons in central New Mexico, with conclusive similarity between ET-θ and β-θ relations. Despite its versatility, the β-θ relation formulated in the literature was largely limited to homogeneous surfaces with localized climate conditions.

For ET over vegetated surfaces, analogous to the bare soil case described by Schlünder, wet patches on surfaces start to develop as the drying front propagates in the vadose zone, creating heterogeneous patterns of water availability and influencing β-θ relation and surface energy exchange. In this study, we extended Schlünder's drying theory over micro-scale bare soil case to macro-scale vegetated surfaces through the analogy between water molecular diffusion and the eddy diffusive convection. A new practical method is proposed to quantify the β-θ relation based on Schlünder's solution to the drying process when the ratio of wet patch radius to the diffusive path is greater than 0.01 (Schlünder 1988a). The wet patch radius is used as an intermediate variable to represent the average size of the wet area over a large vegetated surface, weakening the surface homogeneity assumption used in the P-M method and releasing the dependency on the empirical stomatal resistance terms. The wet patch radius is derived using the statistical analysis on the long-term energy fluxes and soil moisture observations from nine US AmeriFlux sites. The proposed approach aims to provide a physically based yet mathematically tractable method for ET estimation by linking ET, θ, and climate-dependent vegetation covers together via the evolution of wet patch patterns.

MODEL DESCRIPTION

The potential evaporation rate E_p is defined as the ET rate over a large homogeneous area under a given climate condition with unlimited water supply. E_p can be measured through pan evaporation or commonly estimated by the Penman (1948) method. The Penman method was derived based on surface energy balance and the sink strength to calculate evaporation over open waters. It reflects the demand for evaporation, and is used to calculate potential evaporation rate in this study, as:

$$E_p = Q_{ne}\frac{\Delta}{\Delta+\gamma} + E_A\frac{\Delta}{\Delta+\gamma} \quad (1)$$

where Δ is the slope of the saturation vapor pressure curve; γ is the psychrometric constant; Q_{ne} is the ratio of total available energy to latent heat of vaporization; E_A is the drying power of unsaturated air, estimated using the product of air vapor pressure deficit (VPD) and an empirical wind function.

Due to the limited availability of soil water content, the actual ET is usually smaller than E_p over vegetated surfaces under water stress. The derivation from the ideal condition is expressed through a reduction factor (β), which enables the calculation of ET from E_p (Mintz & Walker 1993; Mahfouf *et al.* 1996):

$$\mathrm{ET} = \beta \cdot E_p \quad (2)$$

With limited soil water supply, ET drives the drying process of the top-soil layer. Jointly controlled by atmospheric demand of ET and by internal transport properties of soils, the drying front propagates from the surface to the vadose (unsaturated) zone (Shokri *et al.* 2008, 2012). Schlünder (1988a) described the evaporation process over a partially wetted bare soil surface as the water molecules on the partially saturated area diffuse through the viscous sublayer (Figure 1(a)). The drying process is driven by the vapor pressure deficits among saturation vapor pressure (e^*), vapor pressure at the distance of a patch size (e^0), and the external vapor pressure (e^∞). The Stefan diffusion equation was applied to the two vapor pressure deficit zones to

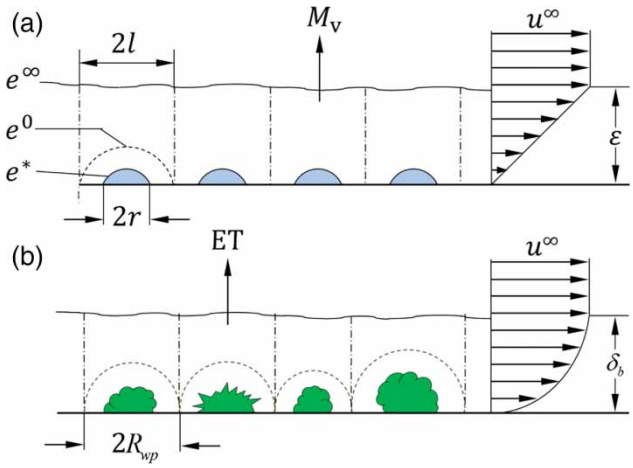

Figure 1 | Diagrams of (a) evaporation over bare soil and (b) ET over vegetated surface. r and l are the radius of the fully and partially wetted patches, respectively; ε is the free path of molecular diffusion; e^* is saturation vapor pressure; e^0 is the vapor pressure at the distance of a partially wetted patch size; e^∞ is the external vapor pressure; u^∞ is the free steam velocity. δ_b is the boundary-layer height.

calculate the actual vapor flux penetrating the area of a single wet patch ($4l^2$). The relative drying rate is obtained by dividing the actual vapor flux by the vapor flux over a fully wetted surface. The detailed derivation of the relative drying rate on bare soil is given by Schlünder (1988b). An approximation of the relative drying rate is given by:

$$\frac{M_v}{M_{v,\mathrm{I}}} = \left[1 + \frac{\pi}{2}\frac{r}{\varepsilon}\sqrt{\frac{\pi}{4\varphi}}\left(\sqrt{\frac{\pi}{4\varphi}} - 1\right)\right]^{-1} \tag{3}$$

where M_v is the actual vapor flux over a wet patch; $M_{\mathrm{v,I}}$ is the vapor flux from a saturated surface; r is the radius of the saturated wet patches (water droplets in Figure 1(a)); ε is thickness of the viscous layer; φ is the relative wetted surface area ($4l^2/\pi r^2$).

ET over the vegetated surface is complicated due to the presence of vegetation in addition to bare soils. Evaporation occurs in soil pores, while transpiration happens inside of the plant stoma with guard cells as additional valves to control the rate of vaporization. The driver of vaporization, VPD is regulated by water availability as well as the external demand due to available energy and turbulent transport efficiency. Ács (2003) investigated the relation between soil moisture to evaporation and transpiration separately, and showed that the difference of evaporation and transpiration is not significant over inhomogeneous surfaces (Ács 2003 Figure 4(b)). Therefore, we attempted to apply Equation (3) over a vegetated surface, with modified wet patch areas reflecting the surface characteristics of vegetation, for eddy diffusive process within the mixing layer. Over vegetated surfaces, as shown in Figure 1(b) in comparison to bare soils, the viscous sublayer height can be replaced by the boundary-layer height (δ_b), the relative wetted surface area is replaced by volumetric soil moisture (θ), and the radius of the saturated area is described as the average wet patch radius (R_{wp}) such that:

$$\beta(R_{wp}, \delta_b, \theta) = \left[1 + \frac{\pi}{2}\frac{R_{wp}}{\delta_b}\sqrt{\frac{\pi}{4\theta}}\left(\sqrt{\frac{\pi}{4\theta}} - 1\right)\right]^{-1} \tag{4}$$

While soil water content (θ) can be readily measured, the determination of δ_b and R_{wp} requires additional effort. When the atmosphere is under neutral condition, the vertical wind profile can be assumed to follow the log-law, i.e.:

$$u_z = \frac{u^*}{\kappa}\ln\left(\frac{z-d}{z_0}\right) \tag{5}$$

where u_z is the wind speed at height z; d is the zero-plane displacement height; z_0 is the roughness height; κ is the Von Kármán constant. Thus, δ_b can be estimated as level (z) that the wind speed increases to free stream velocity (u^∞) (Brutsaert 1982) or as the increase of the wind speed with altitude is relatively small (e.g., $\mathrm{d}u_z/\mathrm{d}z < 0.01$). Here, we aim to estimate ET with physical quantities that are readily measurable in field campaigns, e.g., using eddy covariance (EC) flux towers and soil moisture sensor. To find the estimation of the wet patch radius, the reduction factor was first calculated by Equation (2) using the measured latent heat flux as ET and E_p that was calculated by the Penman method. With soil moisture records and the calculation of δ_b in Equation (5), the wet patch radius can be first estimated by Equation (4). The estimated wet patch radius was statistically regressed on soil moisture to find an analytical curve fitting the data throughout the observation period. The selection was based on the overall goodness of fit R^2. At last, wet patch radius and soil moisture follow an exponential relation as:

$$R_{wp} = c_1 \exp(c_2\theta) \tag{6}$$

where c_1 and c_2 are regression coefficients, which is vegetation type dependent but climate independent. The physical meaning of the coefficients will be discussed in more detail later.

FIELD MEASUREMENT SITES AND DATASET

To test the numerical model proposed in this study, we adopted a dataset obtained from nine EC observation sites from AmeriFlux network. Continuous micrometeorological measurements, including air temperature, humidity, soil water content at two depths (5 cm and 10 cm below the surface), wind speed, sensible heat flux, and latent heat flux, were made at each site. The direct observations were

aggregated into 30-min average time series datasets and published on the AmeriFlux website (http://ameriflux.lbl.gov). The soil water content measurement at the topsoil (0 cm–10 cm depth) that was available was used to represent the surface soil moisture. To account for different vegetation types, the sites were selected based on the main vegetation cover classified by the International Global Biosphere Programme (IGBP) land cover classification system (FRA 2000). The sites primarily contain three types of land cover types, namely, grassland (GRA), closed shrubland (CSH), and evergreen needle leaf forest (ENF) (see Table 1). The locations of the sites were selected across the USA to cover different climate conditions (Figure 2). The mean annual temperatures among the sites vary from 1.5 °C to 21.9 °C, and mean annual precipitations vary from 333 mm to 1,820 mm. Detailed information on the site measurements is listed in Table 1.

RESULTS AND DISCUSSION

The results of correlating the soil moisture and wet patch sizes are shown in Figure 3. With the increase of soil moisture, wet patch radius increases exponentially. For different plant types, the results of regression differentiate from each other as a consequence of different responses of the wet patch radius to the change of soil moisture. The slopes of linear regression, namely c_2 values, dictate the rate of change in R_{wp} to soil wetting/drying processes. Vegetation yielding larger c_2 value has a quicker response to soil moisture change, resulting in rapid change of wet patch radius, and in turn, more rapid change of ET rate. The ET rate of evergreen needleleaf forest is most sensitive to soil moisture content; a similar trend was found in grassland. This result agrees well with the observation by Wolf *et al.* (2014). The change of R_{wp} in response to soil moisture is not significant in shrublands. Living in a water-limited climate, shrubs are less susceptible to water stress and their robust water conserving biophysical functions allow them to sustain water stress for a longer time and to utilize water more efficiently; thus, even with ample soil water supply, shrubs do not fully utilize transpiration capacity for water conservation purpose. The relation between soil moisture and R_{wp} is rather consistent for the specific type in different climate conditions. Thus, type of vegetation is apparently the control parameter if the model is to be applied at different sites.

The comparisons between observations and estimation of hourly ET are shown in Figure 4 for different land cover types. Overall, the ET rate estimated by the proposed method matches with all field observations reasonably well. It is noteworthy that dense plant canopies or large LAI (e.g., forest and grassland) effectively shadow the ground and reduce the amount of available energy impinged on the soil surface (Rothfuss *et al.* 2010). This effect leads to a

Table 1 | Detailed information of AmeriFlux EC sites used in this study

Site name	Land cover (IGBP)	Lat.	Long.	Elev.	Climate classification[a]	Canopy height (m)	Mean annual P (mm)	Mean annual T (°C)	Data period	Reference
Wlr	GRA	37.52	−96.86	408	Cfa	0.3	881	13.5	2001/08/14–2004/09/12	Cook & Coulter (2004)
Goo		34.25	−89.87	87	Cfa	0.3	1,426	15.9	2002/05/06–2006/11/28	Meyers (2006)
KUT		45.00	−93.19	301	Dfa	0.3	777	7.9	2007/08/14–2009/04/30	McFadden (2009)
SO4	CSH	33.38	−116.64	1,429	Csa	2.3	576	13.3	2004/01/05–2006/11/12	Oechel (2019)
FR3		29.94	−97.99	232	Cfa	1.5	869	19.6	2004/07/17–2007/05/25	Heilman (2019)
Rls		43.14	−116.74	1,608	BSh	0.6	333	8.4	2015/04/06–2016/12/21	Flerchinger (2019)
KS1	ENF	28.46	−80.67	1	Cwa	13.0	1,266	21.9	2002/07/15–2003/02/08	Drake & Hinkle (2005)
MRf		44.65	−123.60	263	Csb	25.0	1,820	10.2	2006/04/03–2011/05/01	Law (2019)
NR1		40.03	−105.60	3,050	Dfc	11.5	800	1.5	2005/09/08–2010/10/27	Blanken (2019)

[a]Köppen climate classification (Kottek *et al.* 2006).
Cfa, humid subtropical climate; Dfa, hot-summer humid continental climate; Csa, hot-summer Mediterranean climate; BSh, hot semi-arid climate; Cwa, monsoon-influenced humid subtropical climate; Csb, warm-summer Mediterranean climate; Dfc, subarctic climate.

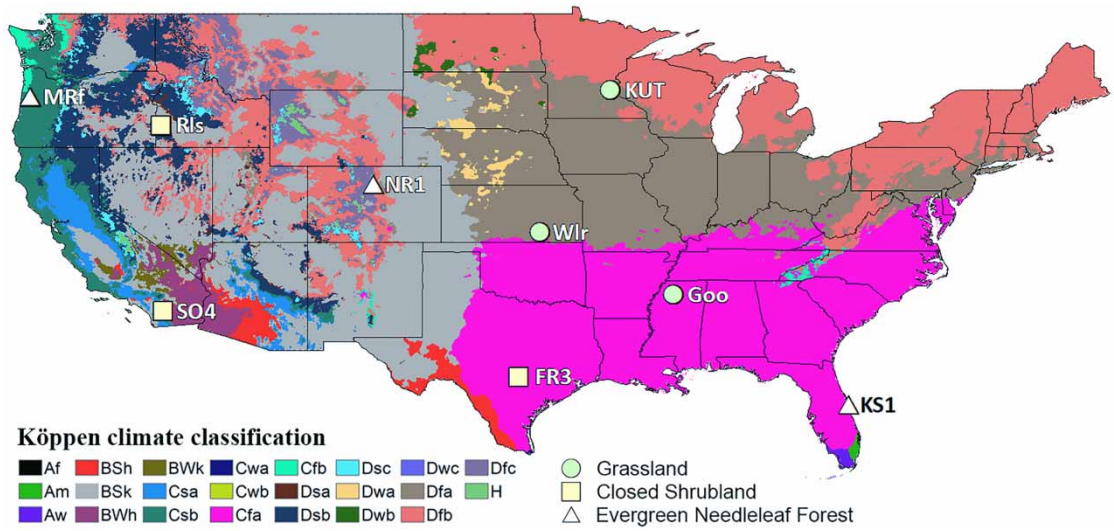

Figure 2 | Locations of selected AmeriFlux EC sites and climate types of the contiguous United States.

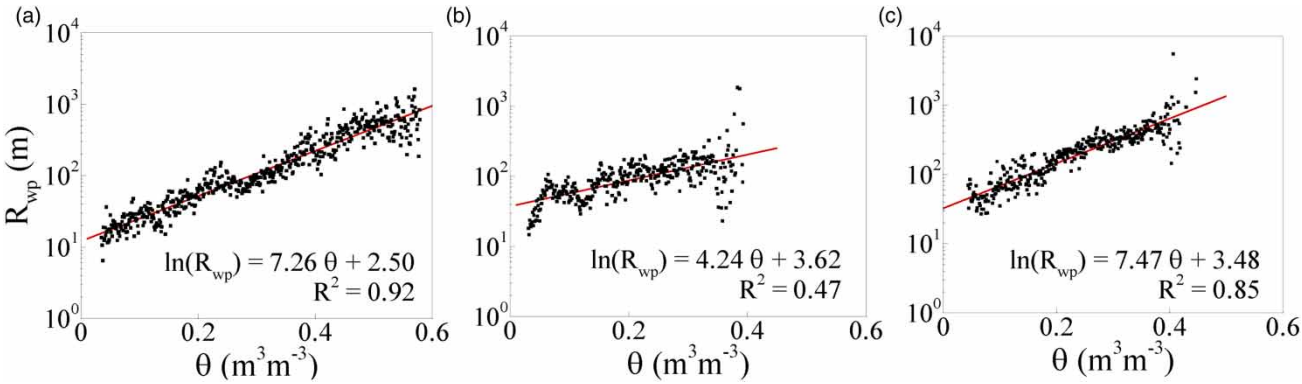

Figure 3 | Exponential relation between soil moisture and R_{wp}: (a) grassland; (b) shrubland; (c) evergreen needleleaf forest. Scattered points are the average wet patch radius for different soil moisture content; the solid lines are the least square regression of the data points for each vegetation category.

consistently transpiration-dominated ET pattern for grasslands and forests over the full range of soil moisture. In contrast, owing to the relatively large fraction of open (exposed) bare soil surface, shrublands experience a shift from plant transpiration to soil evaporation as soil moisture decreases (the threshold at $\theta \sim 0.15$). This shift, in turn, results in less consistency of the ET pattern over shrublands in general, and is responsible for the overall lower goodness of fit (R^2) in the model performance (Figure 4(d)–4(f)). Nevertheless, the realistic quantification of the relation between soil water content and the wet patch size will involve more complex biophysical and environmental determinants of plants, such as plant species, foliage, root water uptake, seasonal variability, and meteorological and geomorphological conditions. Thus, further studies are needed to quantify key parameters and their impact on ET via wet patch sizes and soil water dynamics.

When examining the effect of soil moisture on the reduction factor, their relation shows a high non-linearity and is determined by the ratio of average wet patch radius to constant flux layer height (Figure 5). Qualitatively, the long-term average boundary-layer height is influenced by canopy height and friction velocity in local scale. Its variation is within an order of magnitude from 52 m (over grassland) to 192 m (over forest). The variability of the average wet patch radius is relatively large, from several meters (over dry grassland) to thousands of meters (over wet forest). The change of k, defined as $k = R_{wp}/\delta_b$, is primarily due to

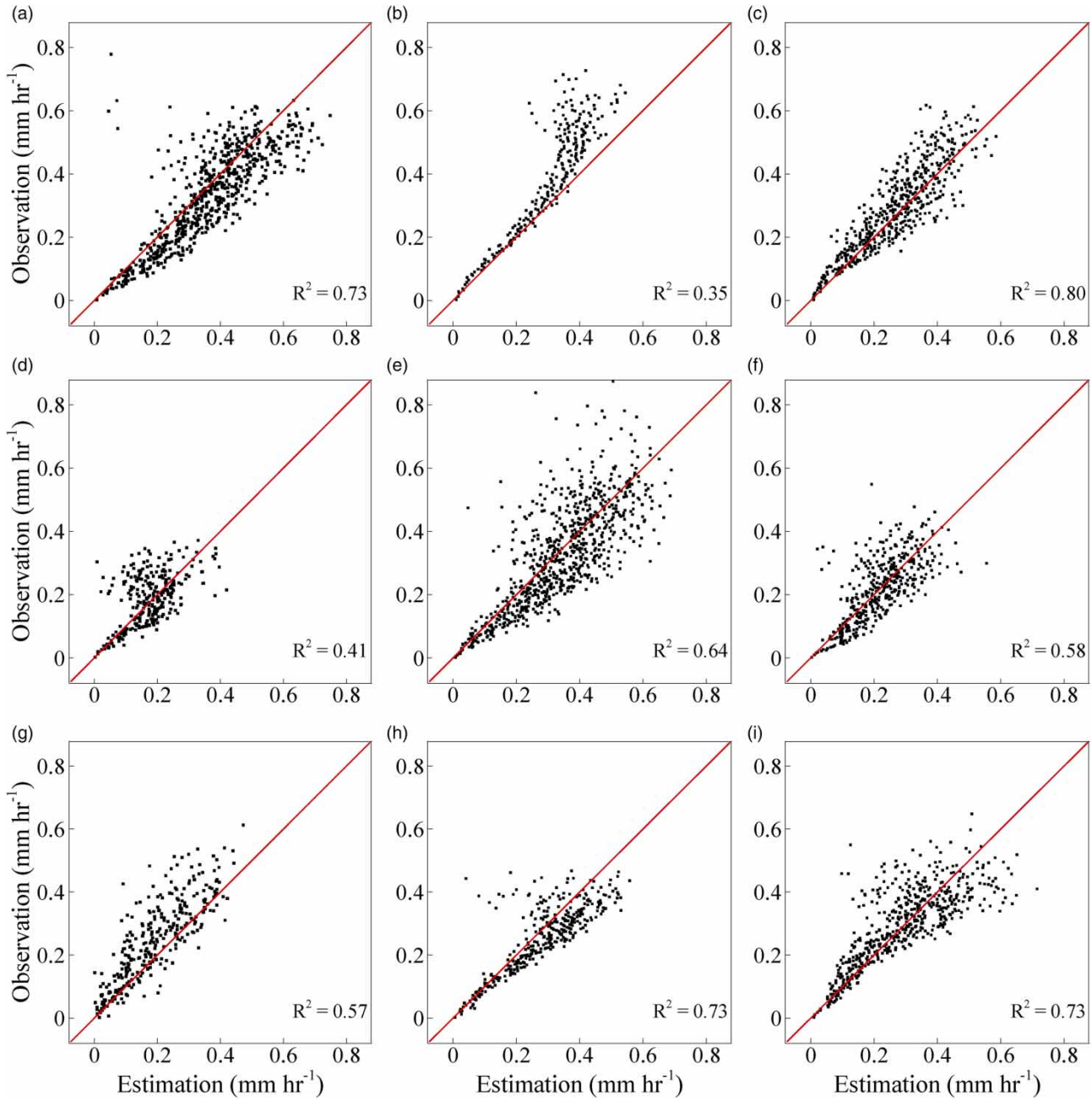

Figure 4 | Results of comparison between observed and estimated ET: grassland (a) Wlr; (b) Goo; (c) KUT; closed shrubland (d) SO4; (e) FR3; (f) Rls; evergreen needleleaf forest (g) KS1; (h) MRf; (i) NR1. The site names follow the definition in Table 1. The scattered points are 30-min averaged ET data.

the change of soil moisture, governed by seasonal precipitation and air humidity. Physically, the parameter k is analogous to the aridity index (potential ET/precipitation) in the Budyko curve, and can be interpreted as a climate dryness index. Small k values represent conditions like arid tropical climate with strong convection in the boundary layer, ample energy supply, but limited precipitation, such that ET is primarily constrained by water availability. In contrast, large k values represent humid climate with excessive precipitation, limited energy supply, and weak turbulent transport. Landscapes with greater annual precipitation and more frequent cloudy days tend to have larger average

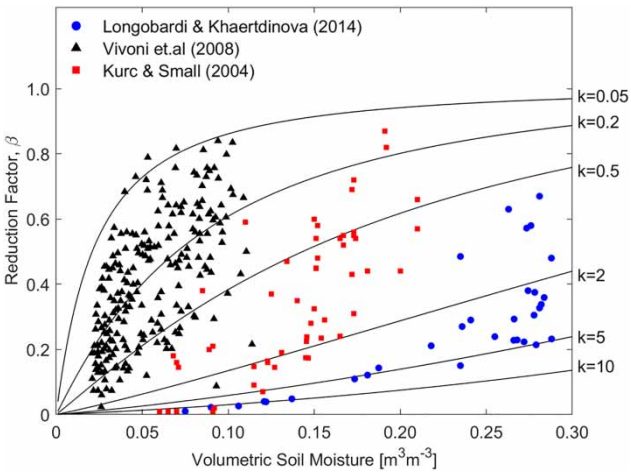

Figure 5 | Relation between θ and β for different $k = R_{wp}/\delta_b$ with the comparison to previous observational studies.

wet patch radius, thus larger k, and vice versa. For small k ($k < 0.2$), the change rate of reduction factor regarding the soil moisture ($d\beta/d\theta$) is much greater when $\theta \sim [0,\ 0.1]$ than it is at larger θ range. The value of β is close to 1 when the surface is humid, indicating smaller k represents a climate with excessive energy supply, high mean temperature, and low chance of rainfall. When k is greater than 2, the reduction factor is smaller than 0.5 with a rather contant $d\beta/d\theta$ over different θ values.

For natural systems, k value can be treated as a climate-dependent or weather-dependent variable. The results are consistent with previous findings. For example, Vivoni *et al.* (2008) monitored ET and soil moisture in the North America monsoon region, where the mean annual temperature is 18 °C and the annual precipitation is 563 mm with a significant seasonal variation. A piece-wise linear function, which was introduced by Laio *et al.* (2001), is used to describe the ET–soil moisture relation in the study. The measurement data points fall between $k = 0.01$ and $k = 0.5$ (Figure 5). Longobardi & Khaertdinova (2014) used ET and soil moisture measurements in southern Italy, which has around 1,000 mm annual precipitation. Most of the data points are in the range of $2 < k < 10$ (Figure 5). In Longobardi & Khaertdinova (2014), a power function relation is suggested for β-θ relation and surface saturation was observed when $\theta \sim 0.28$. In this case, the variation of β largely depends on change of E_p due to energy availability. Kurc & Small (2004) reported cloudy weather will reduce β. The total precipitation over the monsoon period (about three months) is 210 mm, thus the overall measurment has an intermediate range of k.

CONCLUDING REMARKS

In this study, we developed a novel approach for estimating ET based on the soil moisture dynamics in the soil–vegetation–atmosphere continuum, via an intermediate parameter, namely, wet patch radius. A reduction factor that is obtained using an analogy to the solution to the relative drying rate over a partially wetted bare soil surface at pore scale was used to link the actual ET rate to potential ET. The reduction factor was constructed as a function of wet patch radius, the boundary-layer height, and the soil moisture; all can be directly obtained or readily derived from field measurements. In particular, an exponential correlation between soil moisture and the wet patch radius was derived by statistical regression. In general, the ET rate can be characterized by plant types and local climates. The characteristic wet patch radius can be physically interpreted as a spatial pattern of response of different vegetation to water stress.

In practice, the proposed method can be applied by following a rather straightforward procedure. First, by selecting the site where ET is to be estimated, soil moisture content can be obtained from field measurements (be it standalone or as a by-product of flux tower measurement). Partial time series of the soil moisture data (truncated for model calibration) will be needed for estimating the wet patch radius by Equation (6), through regression analysis. The estimated wet patch radius can then be used to find the reduction factor β from Equation (4) in conjunction with the determination of boundary-layer height via wind profile via Equation (5). Lastly, the reduction factor can be applied to the potential ET rate (e.g., using the Penman method in Equation (1) to determine the actual ET). Iteration can be applied to adjust the regression coefficients in the calibration period of the time series to give better model accuracy. Once all model parameters are determined, they can then be applied throughout the rest of the measurement period to estimate the actual ET over the site of interest.

The primary advantage of the proposed method is that it releases the constraint of homogeneity assumption of the

P-M method as well as the dependency on the estimation of stomatal and surface resistance. Yet, it enables users to estimate the actual ET from a parsimonious set of basic micrometeorological variables with reasonable accuracy. In conjunction with remotely sensed data, the framework can be readily extended for high-resolution mapping of ET at regional or continental scales. The model is, nonetheless, sensitive to the landscape characteristics, especially the vegetation type. By resorting to statistical regression for estimating the intermediate (but essential) model parameter, namely, the wet patch radius, the model inherits the limitation and bias of linear regression. A shift of ET pattern between bare soil evaporation and plant transpiration, across some threshold soil water content, can potentially engender inconsistency in model parameter space and lead to degraded model performance. Further study is thus needed to improve the proposed model by incorporating more realistic representation of landscape and environmental determinants, but retaining the simplicity of the fundamental framework.

ACKNOWLEDGEMENTS

The field observations used in this study can be retrieved from AmeriFlux (http://ameriflux.lbl.gov) in 30-min average datasets. The authors acknowledge the following AmeriFlux sites for use of their dataset: US-Wlr, US-Goo, US-KUT, US-SO4, US-FR3, US-Rls, US-KS1, US-MRf, and US-NR1. Funding for AmeriFlux data resources was provided by the U.S. Department of Energy's Office of Science.

REFERENCES

Ács, F. 2003 A comparative analysis of transpiration and bare soil evaporation. *Boundary-Layer Meteorology* **109**, 139–162.

Allen, R., Pereira, L., Raes, D. & Smith, M. 1998 *Crop Evapotranspiration – Guidelines for Computing Crop Water Requirements*. Food and Agriculture Organization of the United Nations, Rome, Italy.

Blanken, P. 2019 *AmeriFlux US-NR1 Niwot Ridge Forest (LTER NWT1)*. doi:10.17190/AMF/1246088.

Brutsaert, W. 1982 *Evaporation Into the Atmosphere: Theory, History and Applications*, 1st edn. Springer, Dordrecht, The Netherlands.

Buckley, T. N. 2017 Modeling stomatal conductance. *Plant Physiology* **174**, 572–582.

Buckley, T. N. & Mott, K. A. 2013 Modelling stomatal conductance in response to environmental factors. *Plant Cell & Environment* **36**, 1691–1699.

Cook, D. & Coulter, R. L. 2004 *AmeriFlux US-Wlr Walnut River Watershed (Smileyburg)*. doi:10.17190/AMF/1246115.

Drake, B. & Hinkle, R. 2005 *AmeriFlux US-KS1 Kennedy Space Center (Slash Pine)*. doi:10.17190/AMF/1246069.

Flerchinger, J. 2019 *AmeriFlux US-Rls RCEW Low Sagebrush*. doi:10.17190/AMF/1418682.

FRA 2000 *Forest Cover Mapping and Monitoring with NOAA-AVHRR and Other Coarse Spatial Resolution Sensors*. Food and Agriculture Organization of the United Nations, Rome, Italy.

Guan, H. & Wilson, J. L. 2009 A hybrid dual-source model for potential evaporation and transpiration partitioning. *Journal of Hydrology* **377**, 405–416.

Guswa, A. J., Celia, M. A. & Rodriguez-Iturbe, I. 2002 Models of soil moisture dynamics in ecohydrology: a comparative study. *Water Resources Research* **38**, 1166.

Haghighi, E. & Kirchner, J. W. 2017 Near-surface turbulence as a missing link in modeling evapotranspiration-soil moisture relationships. *Water Resources Research* **53**, 5320–5344.

Haghighi, E., Shahraeeni, E., Lehmann, P. & Or, D. 2013 Evaporation rates across a convective air boundary layer are dominated by diffusion. *Water Resources Research* **49**, 1602–1610.

Heilman, J. 2019 *AmeriFlux US-FR3 Freeman Ranch-Woodland*. doi:10.17190/AMF/1246055.

Jarvis, P. G. & McNaughton, K. G. 1986 Stomatal control of transpiration: scaling up from leaf to region. *Advances in Ecological Research* **15**, 1–49.

Kottek, M., Grieser, J., Beck, C., Rudolf, B. & Rubel, F. 2006 World map of the Köppen-Geiger Climate Classification updated. *Meteorologische Zeitschrift* **15**, 259–262.

Kumar, R., Jat, M. K. & Shankar, V. 2012 Methods to estimate irrigated reference crop evapotranspiration – a review. *Water Science & Technology* **66** (3), 525–535.

Kurc, S. A. & Small, E. E. 2004 Dynamics of evapotranspiration in semiarid grassland and shrubland ecosystems during the summer monsoon season, central New Mexico. *Water Resources Research* **40**, W09305.

Laio, F., Porporato, A., Ridolfi, L. & Rodriguez-Iturbe, I. 2001 Plants in water-controlled ecosystems: active role in hydrologic processes and response to water stress: II. Probabilistic soil moisture dynamics. *Advances in Water Resources* **24**, 707–723.

Law, B. 2019 *AmeriFlux US-MRf Mary's River (Fir) Site*. doi:10.17190/AMF/1246049.

Lawrence, J. E. & Hornberger, G. M. 2007 Soil moisture variability across climate zones. *Geophysical Research Letters* **34**, L20402.

Lhomme, J. P. & Chehbouni, A. 1999 Comments on dual-source vegetation–atmosphere transfer models. *Agricultural and Forest Meteorology* **94**, 269–273.

Lhomme, J. P., Monteny, B. & Amadou, M. 1994 Estimating sensible heat flux from radiometric temperature over sparse millet. *Agricultural and Forest Meteorology* **68**, 77–91.

Li, S., Zhang, L., Kang, S., Tong, L., Du, T., Hao, X. & Zhao, P. 2015 Comparison of several surface resistance models for estimating crop evapotranspiration over the entire growing season in arid regions. *Agricultural and Forest Meteorology* **208**, 1–15.

Longobardi, A. & Khaertdinova, E. 2014 Relating soil moisture and air temperature to evapotranspiration fluxes during inter-storm periods at a Mediterranean experimental site. *Journal of Arid Land* **7**, 27–36.

Lu, N., Chen, S., Wilske, B., Sun, G. & Chen, J. 2011 Evapotranspiration and soil water relationships in a range of disturbed and undisturbed ecosystems in the semi-arid Inner Mongolia. *China. Journal of Plant Ecology* **4**, 49–60.

Mahfouf, J. F., Ciret, C., Ducharne, A., Irannejad, P., Noilhan, J., Shao, Y., Thornton, P., Xue, Y. & Yang, Z. L. 1996 Analysis of transpiration results from the RICE and PILPS workshop. *Global and Planetary Change* **13**, 73–88.

McFadden, J. 2009 *AmeriFlux US-KUT KUOM Turfgrass Field*. doi:10.17190/AMF/1246145.

Meyers, T. 2006 *AmeriFlux US-Goo Goodwin Creek*. doi:10.17190/AMF/1246058.

Mintz, Y. & Walker, G. K. 1993 Global fields of soil moisture and land surface evapotranspiration derived from observed precipitation and surface air temperature. *Journal of Applied Meteorology* **32**, 1305–1334.

Monteith, J. L. 1965 Evaporation and environment. *Symposia of the Society for Experimental Biology* **19**, 205–234.

Nappo, C. J. 1975 Parameterization of surface moisture and evaporation rate in a planetary boundary layer model. *Journal of Applied Meteorology* **14**, 289–296.

Oechel, W. 2019 *AmeriFlux US-SO4 Sky Oaks-New Stand*. doi:10.17190/AMF/1246099.

Penman, H. L. 1948 Natural evaporation from open water, bare soil and grass. *Proceedings of the Royal Society of London, Series A; Mathematical and Physical Sciences* **193**, 120–145.

Priestley, C. H. B. & Taylor, R. J. 1972 On the assessment of surface heat flux and evaporation using large-scale parameters. *Monthly Weather Review* **100**, 81–92.

Rothfuss, Y., Biron, P., Braud, I., Canale, L., Durand, J.-L., Gaudet, J.-P., Richard, P., Vauclin, M. & Bariac, T. 2010 Partitioning evapotranspiration fluxes into soil evaporation and plant transpiration using water stable isotopes under controlled conditions. *Hydrological Processes* **24**, 3177–3194.

Schlünder, E. U. 1988a On the mechanism of the constant drying rate period and its relevance to diffusion controlled catalytic gas phase reactions. *Chemical Engineering Science* **43**, 2685–2688.

Schlünder, E. U. 1988b Über den Mechanismus des ersten Trocknungsabschnittes und seine mögliche Bedeutung für diffusionskontrollierte katalytische Gasphasen-Reaktionen. (On the mechanism of the constant drying rate period and its relevance to diffusion controlled catalytic gas phase reactions). *Chemie Ingenieur Technik* **60**, 117–120.

Schlünder, E. U. 2004 Drying of porous material during the constant and the falling rate period: a critical review of existing hypotheses. *Drying Technology* **22**, 1517–1532.

Shokri, N., Lehmann, P., Vontobel, P. & Or, D. 2008 Drying front and water content dynamics during evaporation from sand delineated by neutron radiography. *Water Resources Research* **44**, W06418.

Shokri, N., Sahimi, M. & Or, D. 2012 Morphology, propagation dynamics and scaling characteristics of drying fronts in porous media. *Geophysical Research Letters* **39**, L09401.

Shuttleworth, W. J. & Wallace, J. S. 1985 Evaporation from sparse crops – an energy combination theory. *Quarterly Journal of the Royal Meteorological Society* **111**, 839–855.

Thornthwaite, C. W. 1948 An approach toward a rational classification of climate. *Geographical Review* **38**, 55–94.

Thornthwaite, C. W. & Mather, J. R. 1955 The water budget and its use in irrigation. In: *Yearbook Agriculture 1955*. U.S Department of Agriculture, Washington, DC, USA, pp. 346–357.

Vivoni, E. R., Moreno, H. A., Mascaro, G., Rodriguez, J. C., Watts, C. J., Garatuza-Payan, J. & Scott, R. L. 2008 Observed relation between evapotranspiration and soil moisture in the North American monsoon region. *Geophysical Research Letters* **35**, L22403.

Wetzel, P. J. & Chang, J.-T. 1987 Concerning the relationship between evapotranspiration and soil moisture. *Journal of Climate and Applied Meteorology* **26**, 18–27.

Wolf, S., Eugster, W., Ammann, C., Häni, M., Zielis, S., Hiller, R., Stieger, J., Imer, D., Merbold, L. & Buchmann, N. 2014 Corrigendum: contrasting response of grassland versus forest carbon and water fluxes to spring drought in Switzerland (2013 Environ. Res. Lett. 8, 035007). *Environmental Research Letters* **9**, 08950.

Xu, C. Y. & Singh, V. P. 2000 Evaluation and generalization of radiation-based methods for calculating evaporation. *Hydrological Processes* **14**, 339–349.

Xu, C. Y. & Singh, V. P. 2001 Evaluation and generalization of temperature-based methods for calculating evaporation. *Hydrological Processes* **15**, 305–319.

Xue, Y., Sellers, P. J., Kinter, J. L. & Shukla, J. 1991 A simplified biosphere model for global climate studies. *Journal of Climate* **4**, 345–364.

Yang, Y. 2015 *Evapotranspiration Over Heterogeneous Vegetated Surfaces*, 1st edn. Springer-Verlag, Berlin, Heidelberg.

First received 7 March 2019; accepted in revised form 11 May 2019. Available online 31 May 2019